Quantitative proteomics revealed a tight correlation between mitotic phosphorylation/dephosphorylation and structural properties of substrate domains

Hiroya Yamazaki[1], Hidetaka Kosako[2], and Shige H. Yoshimura[1]*

[1]Graduate School of Biostudies, Kyoto University, Kyoto, Japan, [2]Division of Cell Signaling, Fujii Memorial Institute of Medical Sciences, Tokushima University, Tokushima, Japan.

*Corresponding author:
Shige H. Yoshimura
Laboratory of Plasma Membrane and Nuclear Signaling,
Graduate School of Biostudies, Kyoto University,
Yoshida Konoe, Sakyo-ku, Kyoto 606-8501, Japan
Tel & Fax: +81-75-753-7906
E-mail: yoshimura@lif.kyoto-u.ac.jp

Abstract

Protein phosphorylation plays inevitable roles in the regulation and the progression of mitosis. More than ten thousands of phosphorylated residues and their responsible kinases have so far been identified by a number of proteomic analyses. While some of those phosphosites have been demonstrated to affect either protein-protein interaction or catalytic activity of the substrate protein, the effect of most mitotic phosphosites remain unclarified. In this study, we tried to extract structural properties of mitotic phosphosites and neighboring residues, and find a role of heavy phosphorylation at non-structured domain. A quantitative mass spectrometry of mitosis-arrested and non-arrested HeLa cells identified more than 4,100 and 1,900 residues which are significantly phosphorylated, and dephosphorylated at mitotic entry, respectively. Calculating the disorder score of the neighboring amino acid sequence of individual phosphosites revealed that more than 70% of the phosphosites which are dephosphorylated existed in disordered regions, whereas 50% of phosphorylated sites existed in non-structured domain. There was a clear inversed co-relation between probability in non-structured domain and increment of phosphorylation in mitosis. These results indicate that at the entry of mitosis, a significant amount of phosphate group is removed from non-structured domains and attached to more structured domains. GO term analysis revealed that mitosis-related proteins are heavily phosphorylated, whereas RNA-related proteins are both dephosphorylated and phosphorylated, implying that heavy phosphorylation/dephosphorylation in non-structured domain of RNA-binding proteins may play a role in dynamic rearrangement of RNA-containing organelle, as well as other intracellular environments.

Introduction

Protein phosphorylation/dephosphorylation plays critical roles in a number of cellular events such as intracellular signaling, cell cycle regulation, and the progression of mitosis. A number of studies using mass spectrometry successfully identified tens of thousands of phosphorylation sites and drew an entire atlas of phosphorylated states, as well as their dynamic alterations in the cell cycle (1), during mitosis (2) (3) (4), and during cell differentiation and development (5, 6).

The effect of phosphorylation on the structure/function of a substrate protein has been elucidated by various structural biological approaches. An addition of a phosphate group to the hydroxyl group of the target residue (Ser, Thr, or Tyr) affects either i) an interaction with other proteins, ii) the access of a substrate to the catalytic center of the enzyme, or iii) local internal energy, which induces an allosteric effect on the other part(s) of the protein. In any cases, phosphorylation affects stereo-specific interaction between the substrate protein and other molecules, which ensures a tight regulation of biological reactions.

On the other hand, recent bioinformatics studies revealed that phosphorylation preferably occurs at intrinsically disordered regions (IDR) of proteins (7–9). Due to the lack of any secondary and tertiary structures, IDR had been supposed to serve as a flexible substrate not only for phosphorylation, but also for other post-translational modifications (8). Although structural and functional significance of the IDR phosphorylation has not been fully understood, there are some possible explanations. One possibility could be that an addition of phosphate group reduces the flexibility of the IDR, and enables a specific interaction. In a transcription factor Ets1, phosphorylation at a serine residue in IDR changes the structure of the IDR, and reduce the affinity for DNA (10). In regulatory light chain of smooth muscle myosin, phosphorylation at Ser19 in IDR induces the formation of an α-helix, which activates an actin-dependent ATPase activity (11–13).

Another possibility could be the reduction of stereo-specificity between kinase and substrate. Human genome encodes ~520 different kinases and ~150 phosphatases, which phosphorylate or dephosphorylate over 40,000 sites in more than 10,000 proteins (14, 15). It means that a single kinase (a phosphatase) can phosphorylate (dephosphorylate) many different substrate sequences. Indeed, bioinformatic and biochemical studies could identify only weak or no consensus sequences for individual kinases (16) and almost no consensus around the target residue of phosphatases. The existence of the target residue in IDR reduces the stereo-specificity of enzyme-substrate interaction, and enables multiple combinations between them.

Mitosis is one of the most drastic cellular events and is tightly regulated by phosphorylation. At the entry of mitosis, more than several thousands of residues have been known to be phosphorylated (1, 2). A number of kinases which function in mitosis, such as CDK1, Aurora kinase, Plk1, Bub1, and Haspin, etc., have been identified (reviewed in (17–21)). Dephosphorylation also plays essential roles both at the entry and the exit of mitosis (22, 23) (24, 25). More than 1,000 kinds of phosphosites are dephosphorylated during anaphase (26), and more than five hundreds are dephosphorylated at the entry of mitosis (2). For example, CDK1 is activated by dephosphorylation by Cdc25B/C (27, 28), and Cdc25C is partially activated by protein phosphatase

1 (27). These results indicate that a vast number of phosphate groups are transferred to and from the substrate proteins during mitotic entry.

One of the unclarified problems on mitotic phosphorylation could be why and how a vast number of phosphate groups are transferred from a set of proteins to a different set of proteins, and whether these different sets of mitotic phosphosites are structurally different or not. Especially, the distribution of phosphosites in structured or non-structured regions of the substrate proteins is an important cue to understand the structural effect of phosphorylation/dephosphorylation. In this study, we performed phosphoproteomic analysis of cellular proteins to quantify and compare individual phosphosites in mitosis and interphase, and analyzed the structural properties (IDR or structured) of those sites. Analysis of more than 5,000 phosphosites revealed a clear relationship between mitotic phosphorylation/dephosphorylation and IDR.

Result

Quantitative proteomic analysis of phospho-proteins in mitosis

Comparative proteomics was performed on phosphopeptides obtained from asynchronous and mitotic HeLa cells. Tryptic peptides from two populations were labeled with tandem mass tag (TMT) reagents. LC-MS/MS was performed after enrichment of phosphopeptides by TiO_2. Total 17,003 phosophopeptides were quantified (Fig. 1A), and 15,368 of them were assigned to proteins in a database, which are distributed in 3,701 proteins. For quantitative analysis of phophorylation, peptides with only a single phosphosite were extracted and assigned with “mitotic abundance ratio”, which indicates the enrichment of the phosphosite in mitosis over in interphase ($\log_2$(M phase/Asynchronous)). When the phosphosite was detected in more than two different peptides, the abundance ratio was averaged. As a result, 10,255 phosphorylation sites were quantified and were subjected to further analyses, while 4,400 sites were found only in peptides carrying multiple phosphosites. Out of 10,255 sites, 9,656 had already been registered in the phosphoprotein database, PhophoSitePlus (29), indicating our dataset contained ≈600 unreported phosphosites.

To extract phosphosites which are specifically up-regulated or down-regulated in mitosis, the p-value of individual peptides was plotted against the mitotic abundance. Thresholding the p-value at 0.01 (Fig. 1A) could extract two different populations of phosphosites, one in positive and the other in negative in mitotic abundance (Fig. 1B). The positive group (UP group) contains 4,138 phosphosites which distributed in 1,955 proteins, and the negative group (DOWN group) contained 2,249 phosphosites in 1,372 proteins. There was a significant number of proteins (686) which carry both UP and DOWN sites (Fig. 1C). A small peak found at ≈2.4 (Fig. 1B) mainly corresponds to linker domains of C_2H_2 zinc finger proteins, which are known to be phosphorylated in mitosis (30). The mitotic phosphosites, which had been known to be up-regulated, such as S11 and S29 of histone H3.1 (31) and T161 of CDK1 (28), were found in UP group with the abundance ratio of 2.4, 1.3 and 0.8 respectively. The phosphosites known to be down-regulated, such as T14 of CDK1 (28) was found in DOWN group with the mitotic abundance of -0.7.

Gene ontology (GO) analysis was performed for UP and DOWN sites. We obtained the terms of biological process from DAVID (32, 33), and evaluated the enrichment of GO terms in each group of proteins (UP and DOWN sites) by dividing the number of proteins in each group by the total number of proteins in individual GO terms (Fig. 1D). As expected, proteins related to mitotic chromosome were highly enriched in UP sites. Interestingly, proteins related to RNA processing and splicing are highly enriched in both UP and DOWN sites, implying that RNA-related proteins are regulated both by phosphorylation and dephosphrylation in mitosis (see *Discussion*).

The larger number of UP sites than DOWN sites does not necessarily mean that the total amount of phosphorylated proteins in a mitotic cell are larger than dephosphorylated ones. To examine this, the total amount of phosphorylated proteins was quantitated by dot-blot analysis using pIMAGO (34) and compared between interphase and mitosis. Careful quantification revealed that 5.4 fmol of phosphates were attached to proteins in a single mitotic cell, whereas 3.8 fmol in an asynchronous cell. This corresponds to 4.7 and 3.3 mM in a mitotic and an asynchronous cell, respectively (the volume of HeLa cell is supposed to be 1.16 pL (35)), (Fig. S1A), indicating that the amount of phosphate group on proteins are 1.4 times higher in mitotic cells than asynchronous cell. This is concomitant with a decrease of ATP concentration examined by a FRET probe (Fig. S1B, C, E) (36, 37), which was inhibited by a universal kinase inhibitor, staurosporine (Fig. S2A, B). The reduction of the ATP concentration was due neither to the cell swelling during mitosis (38, 39) (Fig. S1D), to the rearrangement of actin cytoskeleton (Fig. S2C, D), nor the reduction of ATP supply (glycolysis and oxidative phosphorylation) (Fig. S2E-H). These results indicate that both phosphorylation and dephosphorylation occur during mitosis, but the amount of phosphorylation dominates over dephosphorylation.

Mitotic dephosphorylation preferably occurs at non-structured regions

The relationship between mitosis-specific phosphorylation/dephosphorylation and higher-order structure of the polypeptides was then investigated. A previous study reported that phosphorylation tends to occur at non-structured region (intrinsically disordered region, IDR) within the substrate protein (7). We evaluated intrinsically disordered score of individual residues by IUPred method (40, 41). In this study, the minimum length of the IDR was set as 30 (see *Materials and Methods*). Under this criterion, 23.4 % of Ser/Thr residues in total cellular proteins exist in IDR (Fig. 2A). On the other hand, 59.6 % of 10,255 phosphosites quantified by our proteomic analysis were assigned in IDR (Fig. 2A), demonstrating a strong tendency of phosphorylation occurring in IDRs.

We then focus on the relationship between mitotic phosphorylation/dephosphorylation and IDR. As shown in Figure 2A, 71.0 % of DOWN and 52.6 % of UP sites exist in IDR. Interestingly, a strong inverse correlation between the abundance ratio and the probability in IDR was found; the IDR probability gradually decreased from ~80 to 40% as the abundance ratio increases (Fig. B). These values are extremely high compared to the average value of all Ser/The residues (23.4 %). These results demonstrate that phosphorylation generally

prefers to occur in IDR, and such preference is significantly strong in dephosphorylation at the entry of mitosis.

The amino acid residue of phosphosites were also tightly co-related to the mitotic abundance ratio. As shown in figure 2C, more than 90 % of DOWN sites are serine, and threonine occupied only ~7.8 %. The percentage of serine reduced as the mitotic abundance increased; 75.2% of UP sites were serine and 24.8 % were threonine. This result indicated that mitotic dephosphorylation occurs mostly at serine residues, whereas mitotic phosphorylation occurs both at serine and threonine. This might be partially related to the high probability of IDR in DOWN sites as demonstrated in Fig. 2A, since serine has higher disorder probability than threonine. Alternatively, this might be due to the preference of phosphatase. PP2A is known to have higher preference for threonine than serine residues, and be inactivated at mitotic entry and re-activated in anaphase as demonstrated previously (3, 23, 26, 42) (see *Discussion*).

Non-conventional sequence motif specific to mitotic phosphorylation

We then analyzed sequence motifs of UP and DOWN sites. The UP and DOWN phosphosites were assigned to one of the following consensus sequences based on their flanking amino acids (from -6 to +6) ; "proline-directed" ([pS/pT]-P), which is phosphorylated by CDK and MAPK, "acidophilic" ([pS/pT]-X-X-[D/E], [pS/pT]-X-[D/E] or [D/E]-X-[pS/pT]), which is recognized by PLK1 and Casein kinase, "basophilic" ([K/R]-X-X-[pS/pT] or [K/R]-X-[pS/pT]), which is phosphorylated by Aurora kinase, PKC, and PKA (2, 43), or "non-conventional", which does not match to any of the three above.

As shown in Figure 3A, B, three conventional motifs ("proline-directed", "acidophilic" and "basophilic") occupied more than 90 % (92.3 %) of DOWN sites, meaning that most of mitotic dephosphorylation occur at one of the conventional motifs. Interestingly, the amount of phosphorylation at non-conventional motifs was higher in UP sites than DOWN sites (Fig. 3A, Fig. S3), suggesting that there could be a mitosis-specific non-conventional motif. The conventional and non-conventional motifs also showed a clear contrast in the relationship between IDR probability and the mitotic abundance. As shown in Figure 3C, the probability in IDR showed inverse correlations to the mitotic abundance ratio in all three conventional motifs, as demonstrated in Figure 2A. In a clear contrast, the IDR probability of non-conventional motif increased as the abundance ratio increased (Fig. 3C). The high IDR probability of UP sites is opposite to the conventional motifs. These results suggest that non-conventional motifs in IDR are phosphorylated in mitosis.

We then analyzed the amino acid sequences of "non-conventional" motif. Logo analysis of 557 UP phospho-serine and 79 UP phospho-threonine in non-conventional motifs found high frequency of basic residues (K or R) at the carboxylic side (+2 - +6) of the phosphosite (Fig. 3D). Especially, K/R at +3 position is distinct. On the other hand, clear consensus was not found at the amino-terminal side of the phosphosite, except for a weak consensus of a hydrophobic residue at -2 position, and K/R at -6 position. This consensus is distinct from any other known kinase motifs, including the conventional basophilic motif, which has basic amino acids at -2 or -3 position. In a clear contrast, such consensus was not found in DOWN sites; 133 DOWN

phospho-serine and 20 DOWN phospho-threonine in non-conventional motifs showed no clear consensus (Fig. 3E). These results suggest that non-conventional basophilic motif is unique for mitotic specific phosphorylation sites.

We conducted GO analysis for proteins carrying UP site in non-conventional motif (502 proteins). In contrast to the GO term analysis for the entire phosphoproteins with UP site, proteins related to "mRNA export from nucleus" are highly enriched in NCB motif (24 out of 502 proteins in non-conventional motif (4.8%) vs. 50 out of 1,955 proteins in entire UP sites (2.6%)) (Fig. 3F). These proteins contain subunits of nuclear pore complex (Nups), splicing factors, and other RNA binding proteins. Nups and proteins with transcription regulator activity are known to carry a substantial amounts of IDRs (44, 45). These results, together with dephosphorylation of RNA related proteins (Fig. 1D), imply that phosphorylation/dephosphorylation of RNA-related proteins play important roles in the progression of mitosis.

Discussion

In this study, we conducted a comparative proteomic analysis of phosphorylated residues in mitosis and interphase cells by using TMT-6plex labeling technique, which can provide the ratio of individual peptide amount in six samples with high precision (46). This approach successfully extracted two different populations of phosphopeptides which are up- or down-regulated at mitotic entry. Bioinformatic analyses of these phosphopeptides revealed a clear correlation between the phosphorylation/dephosphorylation reactions and the IDR probability of the substrate. The most striking outcome of our analysis is that although phosphorylation generally tends to occur in IDR, it is more striking in mitotic dephosphorylation; more than 70 % of DOWN sites exist in IDR, whereas only 50% of UP sites was found in IDR (Fig. 2A, B). This means that as a total, a significant amount of phosphate groups are removed from IDR, and are introduced into more structured regions upon the entry of mitosis. Although the significance of such apparent transition of phosphate groups from IDR to structured regions has not been fully elucidated in this study, several intriguing cues had been obtained from analyses of flanking amino acid sequences and gene ontology. i) Most of mitotic dephosphorylation occur at serine residue (91.9 %), whereas phosphorylation occur at both serine and threonine (75.2%, 24.8 %) (Fig. 2C). ii) proteins involved in mitotic chromosome segregation are heavily phosphorylated, whereas proteins related to RNA splicing, metabolism are both dephosphorylated and phosphorylated (Fig. 1D), iii) a non-conventional basic motif is preferably phosphorylated in mitosis (Fig. 3A, D, E). These results imply an intriguing correlation between mitotic phosphorylation and dynamic higher-order assembly/disassembly of biomolecules (protein, DNA and RNA). The followings are several discussions on the significance of such dynamic behavior of biomolecules in the context of cellular functions.

One of the effects of phosphorylation on IDR could be transition of higher-order structures (10, 47, 48). Phosphorylation in IDR has been known to cause disorder-to-order or order-to-disorder transition. For example, phosphorylation of 4E-BP2 induced the formation of four-stranded β-sheet and prevent the binding

of eIF4E (49). Phosphorylation of phospholamban at Ser16, on the other hand, induced a disruption of higher order structure, which reduced the inhibitory effect of phospholamban on sarco(endo)plasmic Ca-ATPase activity (50, 51).

Another possible effect of phosphorylation at IDR could be that it regulates phase transition of biomolecules. Non-structured polypeptide of IDR has been demonstrated to play a key role for liquid-liquid phase separation (52). It accommodates a number of promiscuous interactions to assemble a number molecules. It was demonstrated that phase transition of protein liquid droplet was induced by phosphorylation/dephosphorylation (53–55). For example, liquid-liquid phase separation of positively charged artificial peptide and RNA complex is promoted by dephosphorylation of the peptide (56). A study using a short hydrophobic peptide which forms hydrogel demonstrated that gel-sol transition could be reversibly induced by phosphorylation-dephosphorylation cycle by kinase and phosphatase (57); the peptide hydrogel was transformed into solution when kinase and ATP was added to the gel, and re-solidified when phosphatase was added to the solution. Such phenomenon was also observed in a living cell. The assembly/disassembly of RNA granules are regulated by phosphorylation/dephosphorylation of one of the subunits (58). Although the mechanism is not fully understood, these lines of evidences imply a possible effect of phosphorylation/dephosphorylation on a dynamic assembly/disassembly transition of biomolecules upon the entry of mitosis. It might be the case that phosphate groups in IDRs weakly assemble the proteins in interphase, and their removal (dephosphorylation) upon the entry of mitosis will induce drastic assembly of the proteins into a stable complex. Alternatively, mitotic phosphorylation solubilizes/disassembles the protein complex, and dephosphorylation in anaphase reassemble them. Indeed, phosphorylation of the proteins in splicing speckle, pericentriolar-satellite and stress granule by DYRK3 disassembled these membraneless organelles in mitosis (59). Such phosphorylation-dependent regulation of protein assembly/disassembly depends on the flanking amino acid sequences of the substrate residue. Previous report demonstrated that the charge pattern, rather than the net charge, was important for phase separation (60). An addition of a minus charge by phosphorylation could enhance or disrupt the charge pattern and affect the progress of phase separation.

Our gene ontology analysis on UP and DOWN phosphosites revealed that RNA-related proteins are preferably dephosphorylated and phosphorylated in mitosis (Fig. 1D). This result is intriguing in the context of phosphorylation-dependent regulation of phase transition in intracellular compartments. Recent studies demonstrated that structure and function of several intracellular compartments are maintained by phase separation, in which RNA plays a role in the molecular assembly (61). P-granule is a cytoplasmic compartment of germ line of C. elegans. P-granule is considered to be liquid-like condensate, which contains mRNA and RNA-binding proteins and may function in posttranscriptional regulation (62, 63). Protein components of P granule, such as PGL-3 and LAF-1, formed liquid droplet *in vtiro*, and mRNA affected the dynamics of these proteins within a droplet (64) (65). Nucleolus is also considered as a compartment, in which proteins and RNAs assembled via mechanism similar to phase separation (66). Nucleolar protein nucleophosmin formed a droplet

with rRNA *in vitro* (67). Phosphorylation at $Thr^{199, 219, 234, 237}$ by CDK1 reduced the affinity for rRNA (68), and replacement of these Ser by Glu partially abolished nucleolar localization in HeLa cells (69), suggesting that phosphorylation of nucleophosmin controls the dynamics of proteins and RNAs within a nucleolus. It might be the case that the removal/addition of a large number of phosphate groups from/to IDRs of RNA-related proteins induces dynamic rearrangements of nucleolus and other RNA-containing nuclear speckles upon the entry of mitosis, which may disrupt these organelle and release a large amount of RNA molecules into the cellular plasm. This will drastically change an intracellular environment, and may affect the assembly/disassembly dynamics of other protein complexes, such as chromosome, which is known to contain preribosomal RNA and nucleolar proteins on the surface (70, 71). It might be the case that chromosome condensation could be induced by orchestrated effects of phosphorylation of chromosome-related proteins (Fig. 1D) and RNA-induced drastic change of an intracellular environment. Further study will be required to elucidate this problem.

It was surprising that most of dephosphorylation at the entry of mitosis occurred at serine, and phosphorylation at both serine and threonine (Fig. 2C), suggesting that threonine phosphorylation is a mitosis-specific event. One of the possible interpretations of such threonine phosphorylation could be that it is coupled with dephosphorylation at anaphase, and therefore involved in temporary phosphorylation of substrate protein during early mitosis. There are several experimental evidences which support this. i) It was demonstrated that dephosphorylation at anaphase and telophase preferably occur at threonine residue in HeLa cells (3, 26). ii) In budding yeast, threonine residues are heavily phosphorylated at the entry of mitosis, and dephosphorylated in anaphase by $PP2A^{Cdc55}$, which is ortholog of $PP2A^{B55}$ (23, 25, 42). iii) Biochemical analysis revealed that $PP2A^{B55}$, one of the major phosphatases working in anaphase, preferably dephosphorylates threonine residues than serine (72). iv) When our dataset of UP site was compared to dephosphorylation dataset previously reported (26), 28.3% of threonine and 16.7% of serine residues were dephosphorylated in anaphase. These lines of evidences suggest that threonine functions as a temporary substrate of phosphorylation, and regulates the reaction which requires tightly-tuned temporal regulation during mitosis. A combination of kinase and phosphatase enables such tight regulation. Although a structural background of threonine-specific reaction is not so far clarified, it must be involved in the early-mitotic events such as chromosome condensation.

We found a mitosis-specific phosphorylation motif, which is similar to conventional basophilic motif but different in the position of basic residues (Fig. 3D). Although it is distinct from any known phosphorylation motifs, several candidates could be found in phosphoproteomic database (2). PKC has been known to function in mitosis (73, 74), and phosphorylate a serine residue near basic amino acids. However, the consensus of several PKC subtypes contain basic residues at C-terminal side as well (43). PKCε plays a role in resolving mitotic DNA catenation (75). Our gene ontology analysis revealed that proteins related to sister chromatid segregation were enriched in proteins carrying NBC motif. Another candidate might be AMPK, which is activated when AMP level increases and ATP level decreases (76), and known to phosphorylates mitosis-related proteins (77). Although primary consensus motif for AMPK is basophilic motif, a peptide carrying K/R at +3

position, which is same as NBC-motif, can also be phosphorylated *in vitro* (78). Out of 243 proteins so far identified as a substrate of AMPK (77), 17.3% (42 proteins) were found as the proteins with UP sites in NBC-motif in our study (Table S1). Furthermore, it is intriguing that the intracellular ATP level decreased during early mitosis (Fig. S1B-D). These results imply the existence of ATP-dependent regulatory mechanism of mitosis; decreased level of intracellular ATP by the activity of conventional kinases at the entry of mitosis may activate AMPK, which then phosphorylates different sets of substrate proteins to proceed the mitotic process. The activity of AMPK increased from early mitosis and began to decrease when starting cytokinesis (77), and this is well match to the ATP level during mitosis (Fig. S1C).

Material and Method

Cell culture and cell synchronization

HeLa cells were cultured in dulbecco's modified eagle medium (DMEM) (SIGMA-aldrich) with 10 % FBS (GIBCO) at 37℃ under 5% CO2. For mitosis arrested cells, we first treated cells with 2 mM thymidine (SIGMA adrich) for 18 hrs. Then cells were washed with PBS (-) and released into DMEM with 10 % FBS for 1 hour. Following treatment with 0.2 μM nocodazole for 10 hours achieved 80% synchronization of HeLa cells at mitosis.

TMT labeling and mass spectrometry

Asynchronous and mitosis-arrested HeLa cells in 100 mm cell culture dish (Corning) were washed twice with 5 mL of ice-cold Hepes-saline (20 mM Hepes-NaOH, pH7.5, 137 mM NaCl). 0.75 mL guanidine hydrochloride buffer (6 M guanidine hydrochloride, 100 mM Tris-HCl (pH8.0), 2 mM DTT) was added, and cell lysates were prepared in triplicate and frozen in liquid nitrogen. The lysates were dissolved by heating and sonication, followed by the centrifugation at 20,000 x g for 15 min at 4^{o}C. The supernatants were reduced in 5 mM DTT at room temperature for 30 min and alkylated in 27.5 mM iodoacetamide at room temperature for 30 min in the dark. Proteins were purified by methanol/chloroform precipitation and solubilized by 25 μL of 0.1% RapiGest SF (Waters) in 50 mM triethylammonium bicarbonate. After repeated sonication and vortex, the proteins were digested with 2 μg of trypsin/Lys-C mix (Promega) for 16 hr at 37^{o}C. Peptide concentration was determined using Pierce quantitative colorimetric peptide assay (Thermo Fisher Scientific). Approximately 150 μg of peptides for each sample were labeled with 200 μg of TMT6-plex reagents (Thermo Fisher Scientific) for 1 hr at room temperature. After the reaction was quenched with hydroxylamine, all the TMT-labeled samples were pooled and acidified with trifluoroacetic acid (TFA). Phosphopeptides were enriched using 50 mg of Titansphere Phos-TiO column (GL Sciences) in accordance with the manufacturer's instructions and then fractionated using Pierce high pH reversed-phase peptide fractionation kit (Thermo Fisher Scientific). Eight fractions were collected using 5%, 7.5%, 10%, 12.5%, 15%, 17.5%, 20%, and 50% acetonitrile (ACN). Each fraction was evaporated in a SpeedVac concentrator and dissolved in 0.1% TFA.

LC-MS/MS analysis of the resultant peptides (1 µg each) was performed on an EASY-nLC 1200 UHPLC connected to a Q Exactive Plus mass spectrometer through a nanoelectrospray ion source (Thermo Fisher Scientific). The peptides were separated on a 75 µm inner diameter × 150 mm C18 reversed-phase column (Nikkyo Technos) with a linear gradient from 4–20% ACN for min 0–180 and 20–32% ACN for min 180–220 followed by an increase to 80% ACN during min 220–230. The mass spectrometer was operated in a data-dependent acquisition mode with a top 10 MS/MS method. MS1 spectra were measured with a resolution of 70,000, an automatic gain control (AGC) target of 3×10^6 and a mass range from 375 to 1,400 *m/z*. HCD MS/MS spectra were acquired at a resolution of 35,000, an AGC target of 1×10^5, an isolation window of 0.4 *m/z*, a maximum injection time of 100 msec and a normalized collision energy of 32. Dynamic exclusion was set to 30 sec. Raw data were directly analyzed against the Swiss-Prot database restricted to *Homo sapiens* using Proteome Discoverer version 2.1 (Thermo Fisher Scientific) with Mascot search engine version 2.5 (Matrix Science) for identification and TMT quantification. The search parameters were (a) trypsin as an enzyme with up to two missed cleavages, (b) precursor mass tolerance of 10 ppm, (c) fragment mass tolerance of 0.02 Da, (d) TMT of lysine and peptide N-terminus and carbamidomethylation of cysteine as fixed modifications, and (e) phosphorylation of serine, threonine and tyrosine, acetylation of protein N-terminus and oxidation of methionine as variable modifications. Peptides were filtered at a false-discovery rate (FDR) of 1 % using the percolator node.

Data analysis

Data analysis was performed by Python2 or 3 and its library (Numpy, Scipy, Pandas, Matplotlib, Seaborn) using Jupyter (IPython) Notebook. The latest version of phosphosites' dataset from PhosphoSitePlus (29) (Wed Nov 08 15:57:30 EST 2017) was used. For GO analysis, DAVID 6.8 (32, 33) was used. The term, "BP_5" was obtained as biological process terms applying homo sapience as a back ground. The number of proteins of our dataset in each term was divided by the total number of proteins in each GO term to evaluate the abundance of the term. For IDR analysis, IUPred method (40, 41) was used. Position-specific estimations of energies of each residue was calculated based on the method in Dosztányi's paper by Perl script. The residues with the energy larger than -0.203 [aeu] were defined as intrinsically disordered residues according to IUPred method. Then the stretch of amino acids with sequence of more than 30 intrinsically disordered residues were regarded as intrinsically disordered region. LOGO analysis of the neighboring amino acids of phosphosites was performed by using "PSP production" algorithm in PhosphoSitePlus (29).

1. Olsen J V, et al. (2010) Quantitative phosphoproteomics reveals widespread full phosphorylation site occupancy during mitosis. *Sci Signal* 3(104):ra3.
2. Dephoure N, et al. (2008) A quantitative atlas of mitotic phosphorylation. *Pnas* 105(31):10762–10767.
3. Malik R, et al. (2009) Quantitative analysis of the human spindle phosphoproteome at distinct mitotic stages. *J Proteome Res* 8(10):4553–4563.
4. Ohta S, Kimura M, Takagi S, Toramoto I, Ishihama Y (2016) Identification of Mitosis-Specific Phosphorylation in Mitotic Chromosome-Associated Proteins. *J Proteome Res* 15(9):3331–3341.
5. Yue J, et al. (2017) Phosphorylation of Pkp1 by RIPK4 regulates epidermal differentiation and skin tumorigenesis. *EMBO J* 36(13):1963–1980.
6. Roux MM, Radeke MJ, Goel M, Mushegian A, Foltz KR (2008) 2DE identification of proteins exhibiting turnover and phosphorylation dynamics during sea urchin egg activation. *Dev Biol* 313(2):630–647.
7. Iakoucheva LM, et al. (2004) The importance of intrinsic disorder for protein phosphorylation. *Nucleic Acids Res* 32(3):1037–1049.
8. Darling AL, Uversky VN (2018) Intrinsic disorder and posttranslational modifications: The darker side of the biological dark matter. *Front Genet* 9(MAY):1–18.
9. Collins MO, Yu L, Campuzano I, Grant SGN, Choudhary JS (2008) Phosphoproteomic Analysis of the Mouse Brain Cytosol Reveals a Predominance of Protein Phosphorylation in Regions of Intrinsic Sequence Disorder. *Mol Cell Proteomics* 7(7):1331–1348.
10. Kasahara K, Shiina M, Higo J, Ogata K, Nakamura H (2018) Phosphorylation of an intrinsically disordered region of Ets1 shifts a multi-modal interaction ensemble to an auto-inhibitory state. *Nucleic Acids Res* 46(5):2243–2251.
11. Nelson WD, Blakely SE, Nesmelov YE, Thomas DD (2005) Site-directed spin labeling reveals a conformational switch in the phosphorylation domain of smooth muscle myosin. *Proc Natl Acad Sci* 102(11):4000–4005.
12. Espinoza-Fonseca LM, Kast D, Thomas DD (2007) Molecular dynamics simulations reveal a disorder-to-order transition on phosphorylation of smooth muscle myosin. *Biophys J* 93(6):2083–2090.
13. Espinoza-Fonseca LM, Kast D, Thomas DD (2008) Thermodynamic and structural basis of phosphorylation-induced disorder-to-order transition in the regulatory light chain of smooth muscle myosin. *J Am Chem Soc* 130(37):12208–12209.
14. Ardito F, Giuliani M, Perrone D, Troiano G, Muzio L Lo (2017) The crucial role of protein phosphorylation in cell signalingand its use as targeted therapy (Review). *Int J Mol Med* 40(2):271–280.
15. Horn H, et al. (2014) KinomeXplorer: An integrated platform for kinome biology studies. *Nat Methods* 11(6):603–604.

16. Rust HL, Thompson PR (2011) Kinase consensus sequences: A breeding ground for crosstalk. *ACS Chem Biol* 6(9):881–892.
17. Bazile F, St-Pierre J, D'Amours D (2010) Three-step model for condensin activation during mitotic chromosome condensation. *Cell Cycle* 9(16):3243–3255.
18. Wang G, Jiang Q, Zhang C (2014) The role of mitotic kinases in coupling the centrosome cycle with the assembly of the mitotic spindle. *J Cell Sci* 127(19):4111–4122.
19. Bayliss R, Fry A, Haq T, Yeoh S (2012) On the molecular mechanisms of mitotic kinase activation. *Open Biol* 2(11):120136–120136.
20. Nigg EA (2001) Mitotic kinases as regulators of cell division and its checkpoints. *Nat Rev Mol Cell Biol* 2(1):21–32.
21. Alvarez-Fernandez M, Malumbres M (2014) Preparing a cell for nuclear envelope breakdown: Spatio-temporal control of phosphorylation during mitotic entry. *BioEssays* 36(8):757–765.
22. Barr FA, Elliott PR, Gruneberg U (2011) Protein phosphatases and the regulation of mitosis. *J Cell Sci* 124(14):2323–2334.
23. Kim H, Fernandes G, Lee C (2016) Protein Phosphatases Involved in Regulating Mitosis: Facts and Hypotheses. *Mol Cells* 39(9):654–62.
24. Sullivan M, Morgan DO (2007) Finishing mitosis, one step at a time. *Nat Rev Mol Cell Biol* 8(11):894–903.
25. Wurzenberger C, Gerlich DW (2011) Phosphatases: Providing safe passage through mitotic exit. *Nat Rev Mol Cell Biol* 12(8):469–482.
26. Castro A, et al. (2015) Global Phosphoproteomic Mapping of Early Mitotic Exit in Human Cells Identifies Novel Substrate Dephosphorylation Motifs. *Mol Cell Proteomics* 14(8):2194–2212.
27. Perdiguero E, Nebreda AR (2004) Regulation of Cdc25C activity during the meiotic G2/M transition. *Cell Cycle* 3(6):733–737.
28. Timofeev O, Cizmecioglu O, Settele F, Kempf T, Hoffmann I (2010) Cdc25 phosphatases are required for timely assembly of CDK1-cyclin B at the G2/M transition. *J Biol Chem* 285(22):16978–16990.
29. Hornbeck P V., et al. (2015) PhosphoSitePlus, 2014: Mutations, PTMs and recalibrations. *Nucleic Acids Res* 43(D1):D512–D520.
30. Rizkallah R, Alexander KE, Hurt MM (2011) Global mitotic phosphorylation of C2H2 zinc finger protein linker peptides. *Cell Cycle* 10(19):3327–3336.
31. Crosio C, et al. (2002) Mitotic Phosphorylation of Histone H3 : Spatio-Temporal Regulation by Mammalian Aurora Kinases. 22(3):874–885.
32. Huang DW, Sherman BT, Lempicki RA (2009) Systematic and integrative analysis of large gene lists using DAVID bioinformatics resources. *Nat Protoc* 4(1):44–57.
33. Huang DW, Sherman BT, Lempicki RA (2009) Bioinformatics enrichment tools: Paths toward the

comprehensive functional analysis of large gene lists. *Nucleic Acids Res* 37(1):1–13.

34. Pan L, et al. (2015) Sensitive measurement of total protein phosphorylation level in complex protein samples. *Analyst* 140:3390–3396.
35. Fujioka A, et al. (2006) Dynamics of the Ras/ERK MAPK cascade as monitored by fluorescent probes. *J Biol Chem* 281(13):8917–8926.
36. Ahn E, Kumar P, Mukha D, Tzur A, Shlomi T (2017) Temporal fluxomics reveals oscillations in TCA cycle flux throughout the mammalian cell cycle. *Mol Syst Biol* 13(11):953.
37. Maeshima K, et al. (2018) A Transient Rise in Free Mg 2+ Ions Released from ATP-Mg Hydrolysis Contributes to Mitotic Chromosome Condensation. *Curr Biol*:1–8.
38. Son S, et al. (2015) Resonant microchannel volume and mass measurements show that suspended cells swell during mitosis. *J Cell Biol* 211(4):757–763.
39. Zlotek-Zlotkiewicz E, Monnier S, Cappello G, Le Berre M, Piel M (2015) Optical volume and mass measurements show that mammalian cells swell during mitosis. *J Cell Biol* 211(4):765–774.
40. Dosztányi Z, Csizmók V, Tompa P, Simon I (2005) The pairwise energy content estimated from amino acid composition discriminates between folded and intrinsically unstructured proteins. *J Mol Biol* 347(4):827–839.
41. Dosztányi Z, Csizmok V, Tompa P, Simon I (2005) IUPred: Web server for the prediction of intrinsically unstructured regions of proteins based on estimated energy content. *Bioinformatics* 21(16):3433–3434.
42. Godfrey M, et al. (2017) PP2ACdc55 Phosphatase Imposes Ordered Cell-Cycle Phosphorylation by Opposing Threonine Phosphorylation. *Mol Cell* 65(3):393–402.e3.
43. Kreegipuu A, Blom N, Brunak S, Ja J (1998) Statistical analysis of protein kinase specifcity determinants. *FEBS Lett* 430:45–50.
44. Patel SS, Denning DP, Fink AL, Uversky V, Rexach M (2003) Disorder in the nuclear pore complex: The FG repeat regions of nucleoporins are natively unfolded. *Proc Natl Acad Sci* 100(5):2450–2455.
45. Haynes C, et al. (2006) Intrinsic disorder is a common feature of hub proteins from four eukaryotic interactomes. *PLoS Comput Biol* 2(8):0890–0901.
46. Hogrebe A, et al. (2018) Benchmarking common quantification strategies for large-scale phosphoproteomics. *Nat Commun* 9(1). doi:10.1038/s41467-018-03309-6.
47. Travers T, et al. (2015) Tandem phosphorylation within an intrinsically disordered region regulates ACTN4 function. *Sci Signal* 8(378):1–10.
48. Fealey ME, Binder BP, Uversky VN, Hinderliter A, Thomas DD (2018) Structural Impact of Phosphorylation and Dielectric Constant Variation on Synaptotagmin's IDR. *Biophys J* 114(3):550–561.
49. Bah A, et al. (2015) Folding of an intrinsically disordered protein by phosphorylation as a regulatory

switch. *Nature* 519(7541):106–9.

50. Metcalfe EE, Traaseth NJ, Veglia G (2005) Serine 16 phosphorylation induces an order-to-disorder transition in monomeric phospholamban. *Biochemistry* 44(11):4386–4396.

51. Chu G, Kranias EG (2003) Functional interplay between dual site phospholambam phosphorylation: insights from genetically altered mouse models. *Basic Res Cardiol* 97(7):1–1.

52. Uversky VN (2017) Intrinsically disordered proteins in overcrowded milieu: Membrane-less organelles, phase separation, and intrinsic disorder. *Curr Opin Struct Biol* 44:18–30.

53. Kwon I, et al. (2014) Phosphorylation-regulated binding of RNA polymerase ii to fibrous polymers of low-complexity domains. *Cell* 156(1–2):374.

54. Guillén-Boixet J, Buzon V, Salvatella X, Méndez R (2016) CPEB4 is regulated during cell cycle by ERK2/Cdk1-mediated phosphorylation and its assembly into liquid-like droplets. *Elife* 5(NOVEMBER2016):1–26.

55. Monahan Z, et al. (2017) Phosphorylation of the FUS low-complexity domain disrupts phase separation, aggregation, and toxicity. *EMBO J* 36(20):e201696394.

56. Aumiller WM, Keating CD (2016) Phosphorylation-mediated RNA/peptide complex coacervation as a model for intracellular liquid organelles. *Nat Chem* 8(2):129–137.

57. Yang Z, Liang G, Wang L, Xu B (2006) Using a kinase/phosphatase switch to regulate a supramolecular hydrogel and forming the supramolecular hydrogel in vivo. *J Am Chem Soc* 128(9):3038–3043.

58. Wang JT, et al. (2014) Regulation of RNA granule dynamics by phosphorylation of serine-rich, intrinsically disordered proteins in C. elegans. *Elife* 3:1–23.

59. Rai AK, Chen JX, Selbach M, Pelkmans L (2018) Kinase-controlled phase transition of membraneless organelles in mitosis. *Nature* 559(7713):211–216.

60. Nott TJ, et al. (2015) Phase Transition of a Disordered Nuage Protein Generates Environmentally Responsive Membraneless Organelles. *Mol Cell* 57(5):936–947.

61. Lin Y, Protter DSW, Rosen MK, Parker R (2015) Formation and Maturation of Phase-Separated Liquid Droplets by RNA-Binding Proteins. *Mol Cell* 60(2):208–219.

62. Updike D, Strome S (2010) P granule assembly and function in Caenorhabditis elegans germ cells. *J Androl* 31(1):53–60.

63. Seydoux G (2018) The P Granules of C. elegans: A Genetic Model for the Study of RNA–Protein Condensates. *J Mol Biol* 430(23):4702–4710.

64. Saha S, et al. (2016) Polar Positioning of Phase-Separated Liquid Compartments in Cells Regulated by an mRNA Competition Mechanism. *Cell* 166(6):1572–1584.e16.

65. Elbaum-Garfinkle S, et al. (2015) The disordered P granule protein LAF-1 drives phase separation into droplets with tunable viscosity and dynamics. *Proc Natl Acad Sci* 112(23):7189–7194.

66. Feric M, et al. (2016) Coexisting Liquid Phases Underlie Nucleolar Subcompartments. *Cell* 165(7):1686–1697.

67. Mitrea DM, et al. (2018) Self-interaction of NPM1 modulates multiple mechanisms of liquid-liquid phase separation. *Nat Commun* 9(1):1–13.

68. Okuwaki M, Tsujimoto M, Nagata K (2002) The RNA Binding Activity of a Ribosome Biogenesis Factor, Nucleophosmin/B23, Is Modulated by Phosphorylation with a Cell Cycle-dependent Kinase and by Association with Its Subtype. *Mol Biol Cell* 13(June):2016–2030.

69. Negi SS, Olson MOJ (2006) Effects of interphase and mitotic phosphorylation on the mobility and location of nucleolar protein B23. *J Cell Sci* 119(17):3676–3685.

70. Van Hooser AA, Yuh P, Heald R (2005) The perichromosomal layer. *Chromosoma* 114(6):377–388.

71. Hayashi Y, Kato K, Kimura K (2017) The hierarchical structure of the perichromosomal layer comprises Ki67, ribosomal RNAs, and nucleolar proteins. *Biochem Biophys Res Commun* 493(2):1043–1049.

72. Pinna LA, Donella-Deana A (1994) Phosphorylated synthetic peptides as tools for studying protein phosphatases. *BBA - Mol Cell Res* 1222(3):415–431.

73. Dai Z, Dulyaninova NG, Kumar S, Bresnick AR, Lawrence DS (2007) Visual Snapshots of Intracellular Kinase Activity at the Onset of Mitosis. *Chem Biol* 14(11):1254–1260.

74. Martini S, et al. (2017) PKCε Controls Mitotic Progression by Regulating Centrosome Migration and Mitotic Spindle Assembly. *Mol Cancer Res*:3–16.

75. Brownlow N, Pike T, Zicha D, Collinson L, Parker PJ (2014) Mitotic catenation is monitored and resolved by a PKC-regulated pathway. *Nat Commun* 5(May):1–13.

76. Hardie DG (2007) AMP-activated/SNF1 protein kinases: Conserved guardians of cellular energy. *Nat Rev Mol Cell Biol* 8(10):774–785.

77. Banko MR, et al. (2011) Chemical Genetic Screen for AMPKα2 Substrates Uncovers a Network of Proteins Involved in Mitosis. *Mol Cell* 44(6):878–892.

78. Gwinn DM, et al. (2008) AMPK Phosphorylation of Raptor Mediates a Metabolic Checkpoint. *Mol Cell* 30(2):214–226.

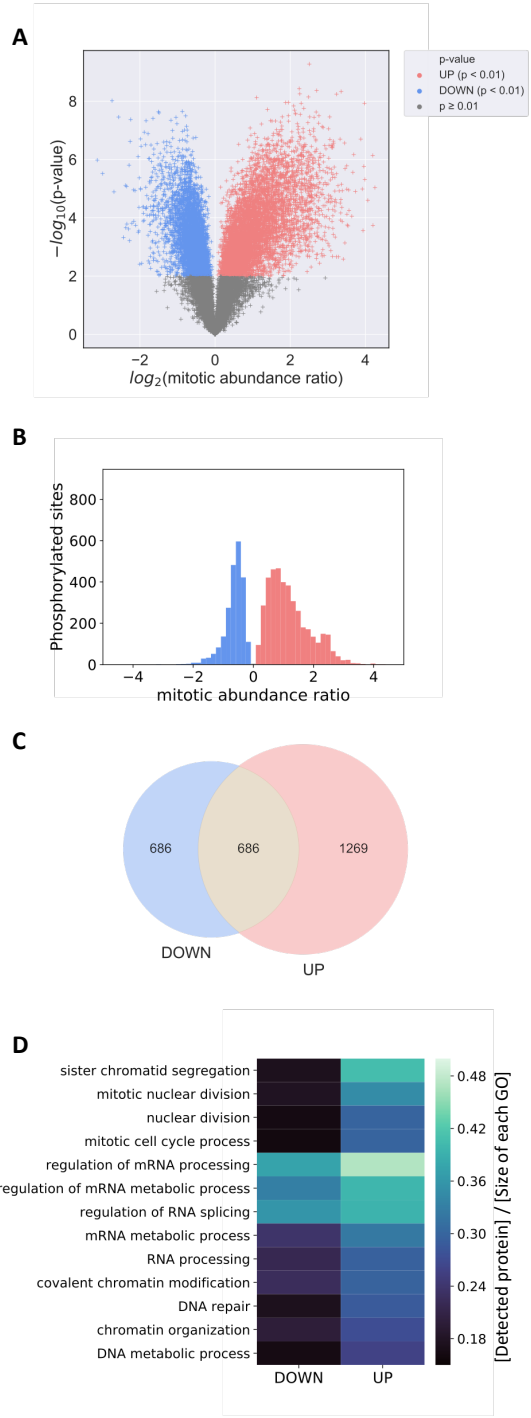

Yamazaki et al. Figure 1

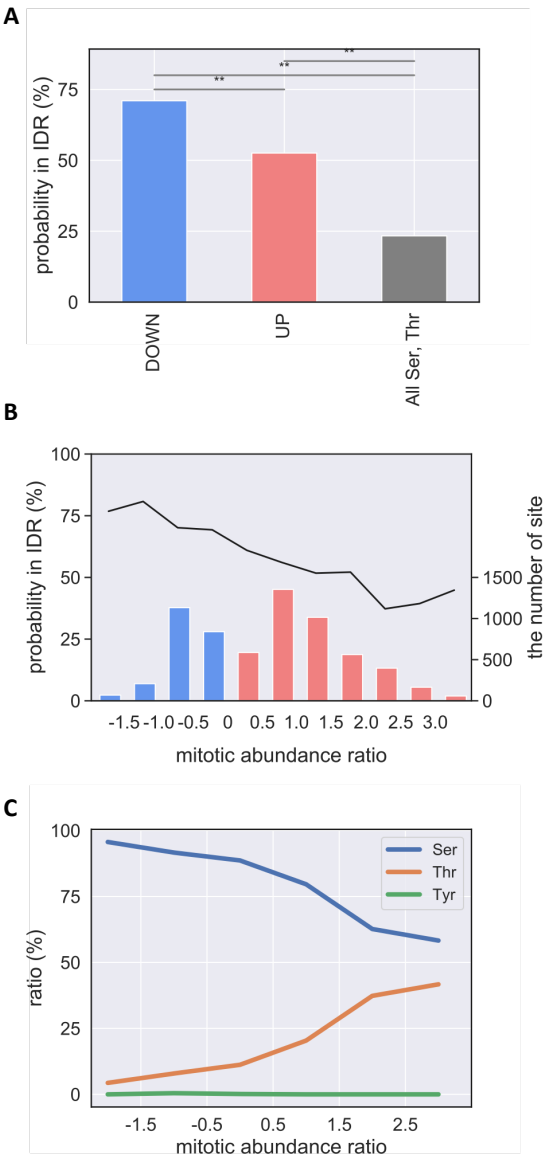

Yamazaki et al. Figure 2

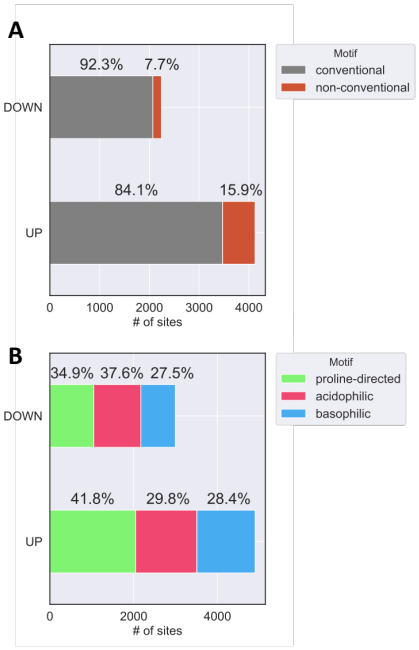

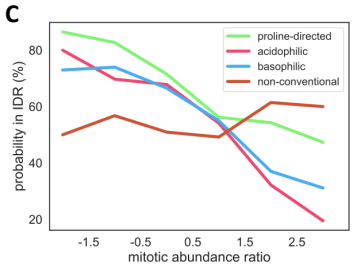

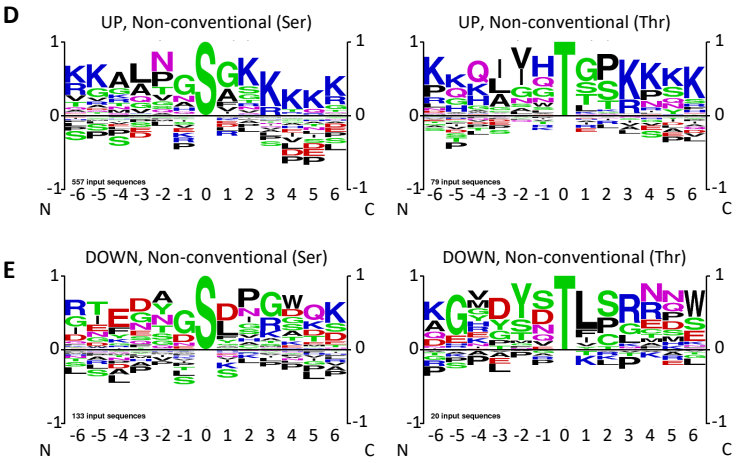

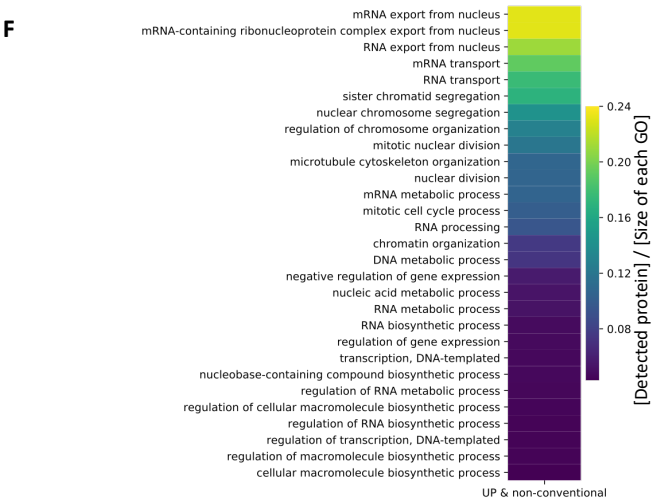

Yamazaki et al. Figure 3

Figure and Figure Legends

Figure 1. Quantification of mitotic phosphorylation by tandem mass tag analysis

(A) A volcano plot of TMT-analysis. The p-value and the abundance ratio of individual phosphopeptides were plotted. The peptides with the p-value lower than 2 (grey) were eliminated from the subsequent analyses. The peptides with positive (red) and negative (blue) were extracted and were subjected to the subsequent analyses.
(B) Histogram of the abundance ratio. UP (red) and DOWN (Blue) sites are distinguished.
(C) Venn diagram of the number of proteins carrying UP and/or DOWN sites.
(D) Gene ontology analysis of phosphoproteins carrying UP or DOWN sites. Biological process term were obtained from DAVID. The number of proteins identified in this study was divided by the number of total proteins in each term. Shown here are several terms relatively abundant UP and DOWN sites.

Figure 2. Structural properties of mitotic phosphosites.

(A) The probability of phosphosites existing in intrinsically disordered regions. The IDR probabilities of all serine and threonine residues, all phosphosites, UP sites and DOWN sites are plotted.
(B) The relationship between IDR probability and the abundance ratio.
(C) The relationship between the amino acid residue of phosphosites and the abundance ratio.

Figure 3. Neighboring sequences of mitotic phosphosites

(A, B) The ratio of conventional and non-conventional motifs (A) and the ratio of individual conventional motifs (B) in UP and DOWN sites.
(C) The relationship between the IDR probability and the abundance ratio was analyzed for individual conventional motifs and non-conventional motif.
(D, E) Logo analysis of flanking residues of UP (D) and DOWN (E) sites in non-conventional motif. The results for phosphoserine (left) and phosphothreonine (right) are shown.
(F) Gene ontology (biological process) analysis on proteins with UP sites in non-conventional motif. The number of proteins identified was divided by the total number of proteins in each term.

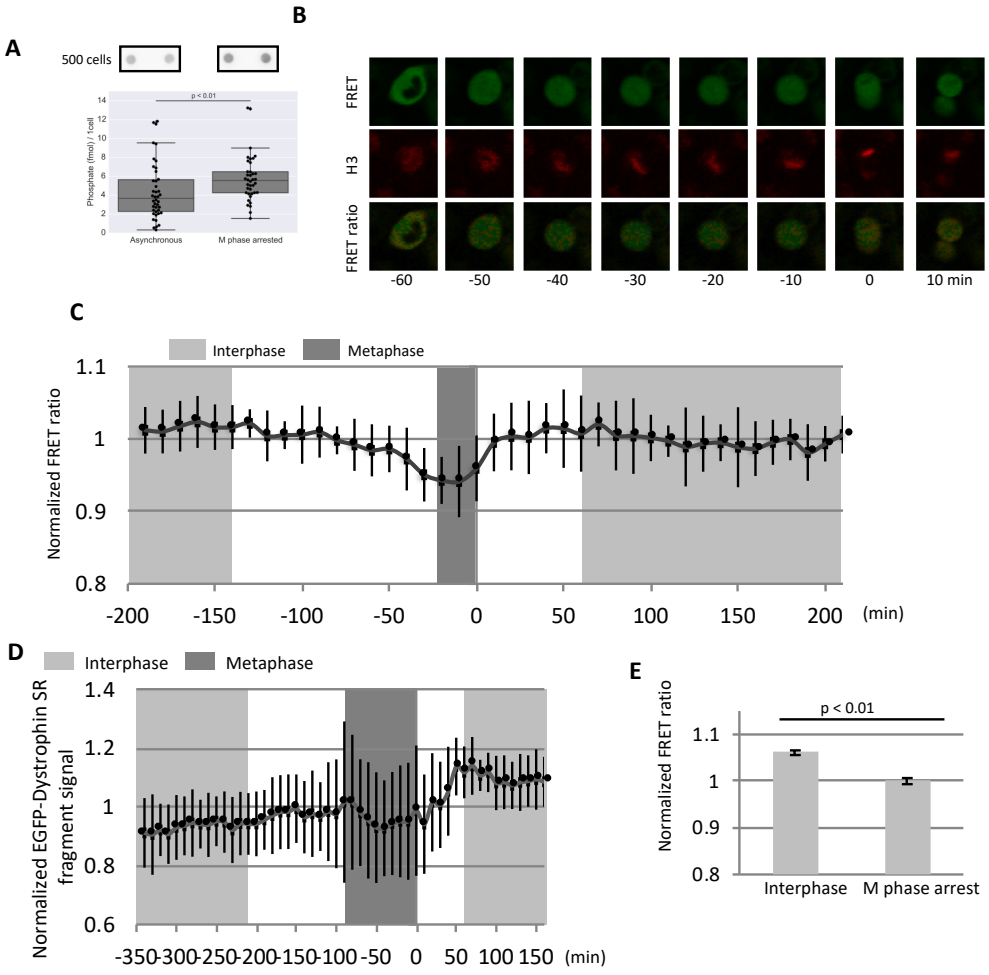

Yamazaki et al. Figure S1

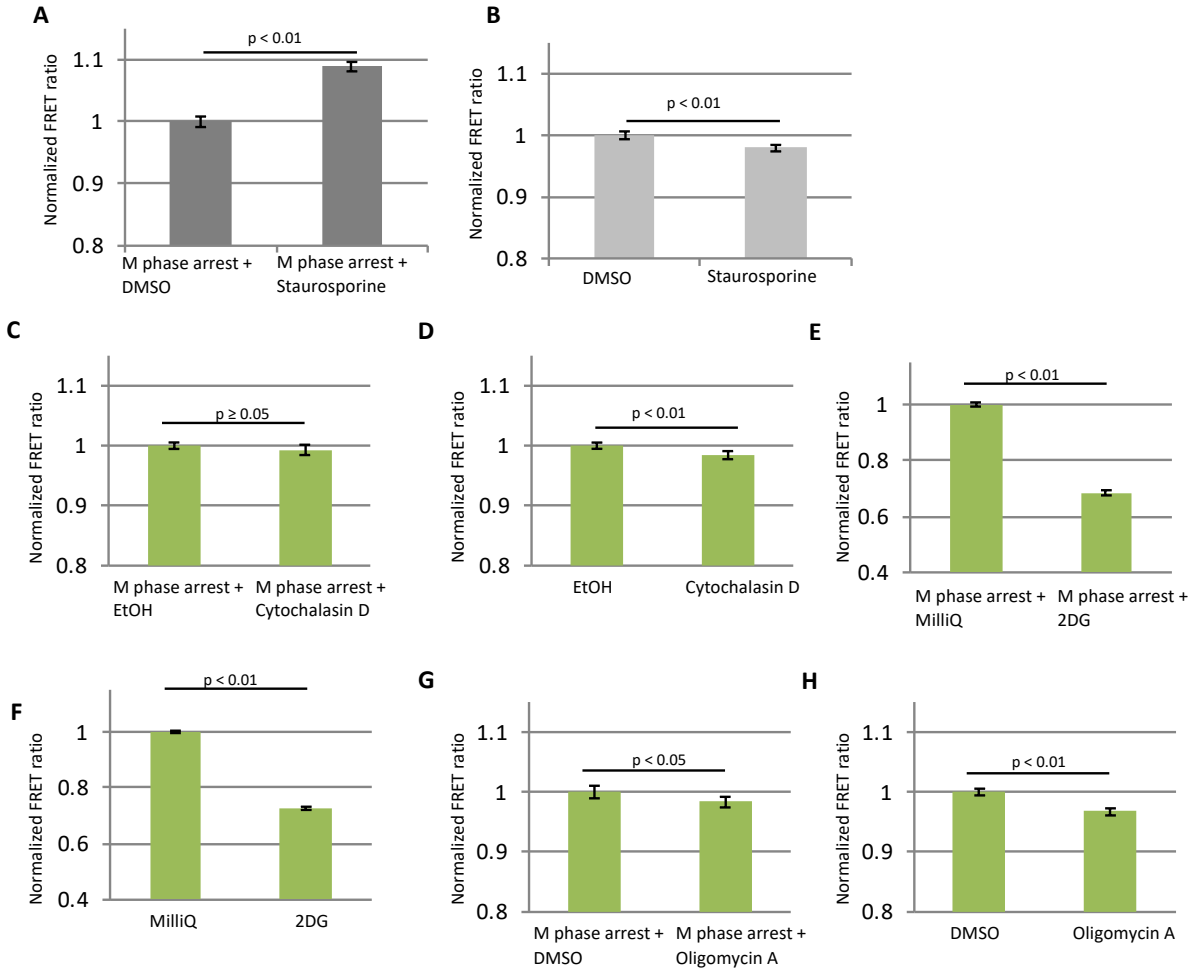

Yamazaki et al. Figure S2

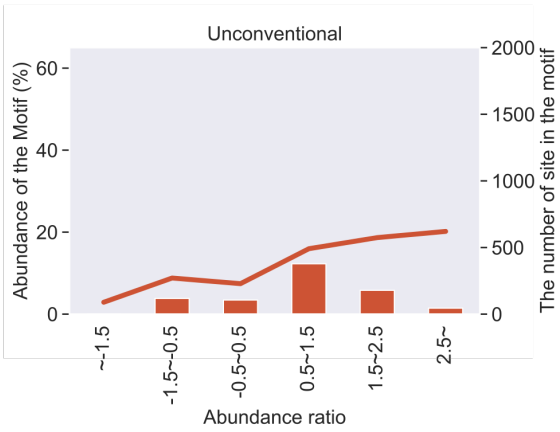

Yamazaki et al. Figure S3

Supplemental Figure, Table and Legends

Figure S1. Total amount of phosphoprotein increases and intracellular ATP level decreases during mitosis.

(A) The amount of phosphate on proteins in asynchronous and nocodazole-treated HeLa cells was quantified using pIMAGO and streptavidin HRP conjugate. Dot-blot analysis of the cell lysate from 500 cells is shown here. The data points are obtained from three independent experiments and outlier was eliminated at each experiment using method of a function of the inter-quartile range. The significance was tested by Mann–Whitney U-test.

(B, C) Quantification of the cytoplasmic ATP level during mitosis. HeLa cells expressing ATeam and mPlum-Histone H3 were observed by live-cell time-lapse imaging. Representative fluorescence images of FRET signal, mPlum signal and acceptor/donner ratio are shown (B). Time 0 is defined when chromosomes started to segregate at anaphase onset. The acceptor/donner ratio was quantified in images, normalized to that in interphase, and plotted against time (C). Data was collected from 16 cells and each data points has at least 8 cells. Error bars represents S.D.

(D) The experiment described in Fig S1B was performed with EGFP-tagged dystrophin. Data was collected from 13 cells and each data points has at least 7 cells. Error bars represent S.D.

(E) Comparison of cytoplasmic ATP level between non-treated and nocodazole-treated HeLa cells. HeLa cells expressing ATeam were treated with 2 mM thymidine for 18 hours and released to DMEM with 10% FBS for 1 hour. Then cells were treated with or without 0.2 μM nocodazole for 10 hours, and observed by confocal fluorescence microscopy. The acceptor/donner ratio was quantified in the obtained images and summarized. Data was collected from more than 100 cells. The value was normalized by that of nocodazole-treated cells. The reduction of signal in mitosis was observed as is the case in living cells shown in B and C. Error bars represent 95% CI. The significance was tested by Welch's t-test.

Figure S2. Protein phosphorylation decreases the intracellular ATP level during mitosis.

The experiment described in Fig. S1D was performed in the presence of various inhibitors in M-phase arrested cells (A, C, E, G) and non-synchronized cells (B, D, F, H). For M-phase arrest, HeLa cells were treated with thymidine for 18 hours, and, after incubation with normal medium for 1 hour, treated with 0.2 μM nocodazole for 10 hours.

(A, B) Cells were treated with 1 μM Staurosporine, an inhibitor of for 1 hour.

(C, D) Cell were treated with 1 μM Cytochalasin D, an inhibitor of actin polymerization, for 1 hour.

(E, F) Cells were treated with 10 mM 2-deoxy-D-glucose (2DG), an inhibitor of glycolysis for 1 hour.

(G, H) Cells were treated with12.6 μM Oligomycin A, an inhibitor of oxidative phosphorylation, for 1 hour.

The acceptor/donner ratio was quantified in the obtained images, and normalized by that in the absence of the inhibitor. Error bars represent 95% CI. The significance was tested with Welch's t-test.

583

584 **Figure S3. Occupancy of non-conventional motif against early mitotic abundance ratio**

585 The occupancy of sites in non-conventional motif was increase along with early mitotic abundance ratio

586

587 **Table S1. Proteins with UP non-conventional motif, which are phosphorylated by AMPK.**

588 42 proteins with UP non-conventional motif have been identified as the substrates of AMPK in previous

589 report.